The AAPS Journal (2019) 21: 43
DOI: 10.1208/s12248-019-0314-1

Check for updates

Research Article

Theoretical Considerations for Direct Translation of Unbound Liver-to-Plasma Partition Coefficient from *In Vitro* to *In Vivo*

Zhenhong Li,[1,3] Li Di,[2] and Tristan S. Maurer[1]

Received 31 October 2018; accepted 26 February 2019; published online 18 March 2019

Abstract. There is considerable interest in developing methods to predict the asymmetric distribution of unbound drug into tissues. The liver is of particular interest due to the multitude of expressed transporters with potential implications for pharmacokinetics, pharmacodynamics, and toxicology. Empirical correlations of *in vitro* unbound hepatocyte-to-media partition coefficient (*in vitro* K_{puu}) and *in vivo* unbound liver-to-plasma partition coefficient (*in vivo* K_{puu}) have been reported without considering the theoretical aspects which might confound the interpretation of such observations. To understand the theoretical basis for the translation of K_{puu} between *in vitro* and *in vivo* systems, we simulated *in vitro* hepatocyte and *in vivo* liver K_{puu} values using mechanistic mathematical models of these systems. Theoretical comparisons of steady-state K_{puu} between *in vitro* and *in vivo* systems were performed using liver models which assumed a number of segments ranging from one (*i.e.*, a permeability-limited well-stirred model) to infinity (*i.e.*, a permeability-limited parallel tube model). Using a five-segment model, the effect of zonal differences in metabolism was also explored in this context. The results across the range of examined models indicated that theoretical differences between *in vitro* and *in vivo* K_{puu} estimates exist and are expected to increase with an increasing degree of extraction across the liver. However, differences were relatively small using what is perhaps the most physiologically relevant, permeability-limited parallel tube model, suggesting that direct correlations are reasonably valid and that the permeability-limited parallel tube model is perhaps the most appropriate physiologically based pharmacokinetic (PBPK) construct for supporting studies of this nature.

KEY WORDS: extended clearance model; five-compartment model; IVIVE; K_{puu}; parallel tube model.

INTRODUCTION

Liver-to-plasma unbound partition coefficient (K_{puu}) provides useful information regarding the unbound drug concentration ratio between the liver and the plasma and is important for quantitative prediction of efficacy and toxicity of intracellular targets. For drugs that are substrates of active uptake transporters, intracellular unbound drug concentrations may be higher than those in the plasma; so unbound plasma concentrations may lead to an underestimation of the potential for efficacy and toxicity in the liver. In contrast, intracellular unbound drug concentrations may be lower than those in the plasma for efflux transporter substrates, so that unbound plasma drug concentrations can overestimate liver efficacy and toxicity.

For these reasons, a number of *in vitro* assays have been developed to estimate the hepatocyte K_{puu}*in vitro* including the binding method (1–3), temperature method (4), and the kinetic method (5). Recently, we reported an *in vitro-in vivo* correlation (IVIVE) for liver-to-plasma K_{puu} for a small number of compounds along the line of unity using cryopreserved suspension rat or human hepatocytes from multiple donors in the presence of 4% BSA (3), which infers that the drug-metabolizing enzymes and transporters are functioning at levels consistent with those *in vivo*. Of course, the broader predictive utility of such systems and strength of such associated physiological and mechanistic inference depend upon the assumed theoretical translatability between *in vitro* and *in vivo* systems. Theoretical issues relating to differing conditions at the time of sampling (*e.g.*, steady state *vs.* pseudo-steady state), differing sites of sampling (*e.g.*, systemic *vs.* hepatic blood), differing dosing

Electronic supplementary material The online version of this article (https://doi.org/10.1208/s12248-019-0314-1) contains supplementary material, which is available to authorized users.

[1] Medicine Design Modeling and Simulation, Pfizer Inc., 1 Portland St. Pfizer, Cambridge, Massachusetts 02139, USA.
[2] Pharmacokinetics, Dynamics and Metabolism, Pfizer Inc., Groton, Connecticut, USA.
[3] To whom correspondence should be addressed. (e–mail: zhenhong.li@pfizer.com)

routes (*e.g.*, IV *vs*. PO), and differing physiological processes between systems (*e.g.*, enterohepatic recirculation) may challenge the validity of conclusions derived from such empirical correlations and erode confidence in the general predictive utility of *in vitro* systems.

To understand the theoretical basis for the direct K_{puu} translation, we utilized several common physiologically based pharmacokinetic (PBPK) models of *in vitro* (Fig. 1a) and *in vivo* (Fig. 1b, c) systems. For the liver, model structures employed a number of permeability-limited liver segments (Fig. 1c), with each further split into one liver tissue and one liver blood sub-compartment (Fig. 1b). The number of liver segments ranges from one to infinity (essentially a permeability-limited parallel tube model). Formulas that translate K_{puu} from *in vitro* to *in vivo* were derived from each model, and simulations were performed to evaluate such correlations over a range of hepatic extraction ratios (ER). In addition, the impact of zonation in metabolic clearance was examined. The results are shown to be consistent with previous publications and provide theoretically based insight into the validity and limitations of empirical *in vitro-in vivo* K_{puu} correlations.

METHODS

To compare mathematical expressions of *in vitro* and *in vivo* K_{puu}, we assumed that all the transporters, enzymes, and passive permeation processes in the *in vitro* assay were maintained well through the incubation time (6) and functioning at the same rates as those *in vivo*. As such, after being scaled to the number of hepatocytes, passive permeation into hepatocytes ($CL_{p,in}$), passive permeation out of hepatocytes ($CL_{p,out}$), active uptake into hepatocytes (CL_{up}), efflux out of hepatocytes (CL_{eff}), biliary clearance (CL_{bil}), and metabolic clearance (CL_{met}) in the *in vitro* and *in vivo* systems are all the same with a unit of microliters per minute per million hepatocytes. Although it is quite controversial if transporters and enzymes *in vitro* operate as efficiently as *in vivo* (7–14), this is a necessary hypothesis to simplify the question and allow us to examine the theoretical discrepancy between *in vitro* and *in vivo* K_{puu}. In addition, clearance rates in all equations mentioned above and in the following are based on unbound drug concentrations.

Derivation of a Mathematical Expression for *In Vitro* K_{puu}

The equation of *in vitro* K_{puu} was derived under the assay conditions using suspension hepatocytes. Details of this assay have been published previously (3). In summary, 0.5 million cryopreserved suspension hepatocytes were incubated with 1 μM test compound in 1 mL InVitroGRO HI media supplemented with 4% BSA for 4 h to achieve steady state. The total extracellular concentration (C_{ec}), total intracellular concentration (C_{ic}), and fraction of unbound drugs in cells ($f_{u,ic}$) and in media ($f_{u,ec}$) were measured (2) to calculate free drug concentrations in hepatocytes and media, from which *in vitro* K_{puu} was obtained (Eq. 1).

$$K_{puu,invitro} = \frac{C_{ic} \times f_{u,ic}}{C_{ec} \times f_{u,ec}} \quad (1)$$

In the assay (Fig. 1a), compounds enter hepatocytes through both passive permeation and active transport, which are also the two mechanisms for compounds leaving the cells. However, the passive permeation and active transport from media to cells could be different than those from cells to media. As a result, processes of $CL_{p,in}$, $CL_{p,out}$, CL_{up}, CL_{eff}, CL_{bil}, and CL_{met} were included in Eqs. 2 and 3 to describe the kinetics of C_{ec} and C_{ic}. Bile canaliculi were not present in the *in vitro* assay; however, both biliary and basolateral efflux transporters were assumed to function as those *in vivo* with drug returned to the media through CL_{eff} and CL_{bil} rather than being eliminated. In addition, CL_{met} was assumed to occur only intracellularly.

$$\frac{dC_{ec} \times V_m}{dt} = \left(CL_{p,out} + CL_{eff} + CL_{bil}\right) \times C_{ic} \times f_{u,ic} - \left(CL_{p,in} + CL_{up}\right) \times C_{ec} \times f_{u,ec} \quad (2)$$

$$\frac{dC_{ic} \times V_c}{dt} = \left(CL_{p,in} + CL_{up}\right) \times C_{ec} \times f_{u,ec} - \left(CL_{p,out} + CL_{met} + CL_{bil} + CL_{eff}\right) \times C_{ic} \times f_{u,ic} \quad (3)$$

In Eqs. 2 and 3, V_m and V_c represent the volumes of media and cells, respectively. If CL_{met} is not zero, this system can only produce a pseudo-steady-state (PSS) condition when *in vitro* K_{puu} was obtained. Under the PSS condition, both C_{ic} and C_{ec} decline with the same first-order rate constant (k_{deg}), yielding a constant ratio of their concentrations that is then converted to *in vitro* K_{puu} after $f_{u,ic}$ and $f_{u,ec}$ being considered (Eq. 1). The determinants of this measurement are unclear and likely to differ from that previously published under the assumption of a true steady state (TSS) condition (2) (Eq. 4).

$$K_{puu,invitro,\ TSS} = \frac{CL_{p,in} + CL_{up}}{CL_{p,out} + CL_{bil} + CL_{eff} + CL_{met}} \quad (4)$$

To better understand the potential difference between the TSS and PSS $K_{puu,\ in\ vitro}$, we developed a mathematical expression of the PSS $K_{puu,\ in\ vitro}$, which also facilitates a better understanding of the theoretical translatability of this *in vitro* measurement.

In the first step, we defined the rate of change of the total amount of drug within the system via the summation of Eqs. 2 and 3 (Eq. 5), leading to an algebraic representation of k_{deg} (Eq. 6). Likewise, under PSS conditions, Eq. 3 can be rewritten to Eq. 7, using k_{deg} to formulate the rate of change in total intracellular amount. Equation 8 is then derived to represent the measured PSS $K_{puu,\ in\ vitro}$ that equals Eq. 1.

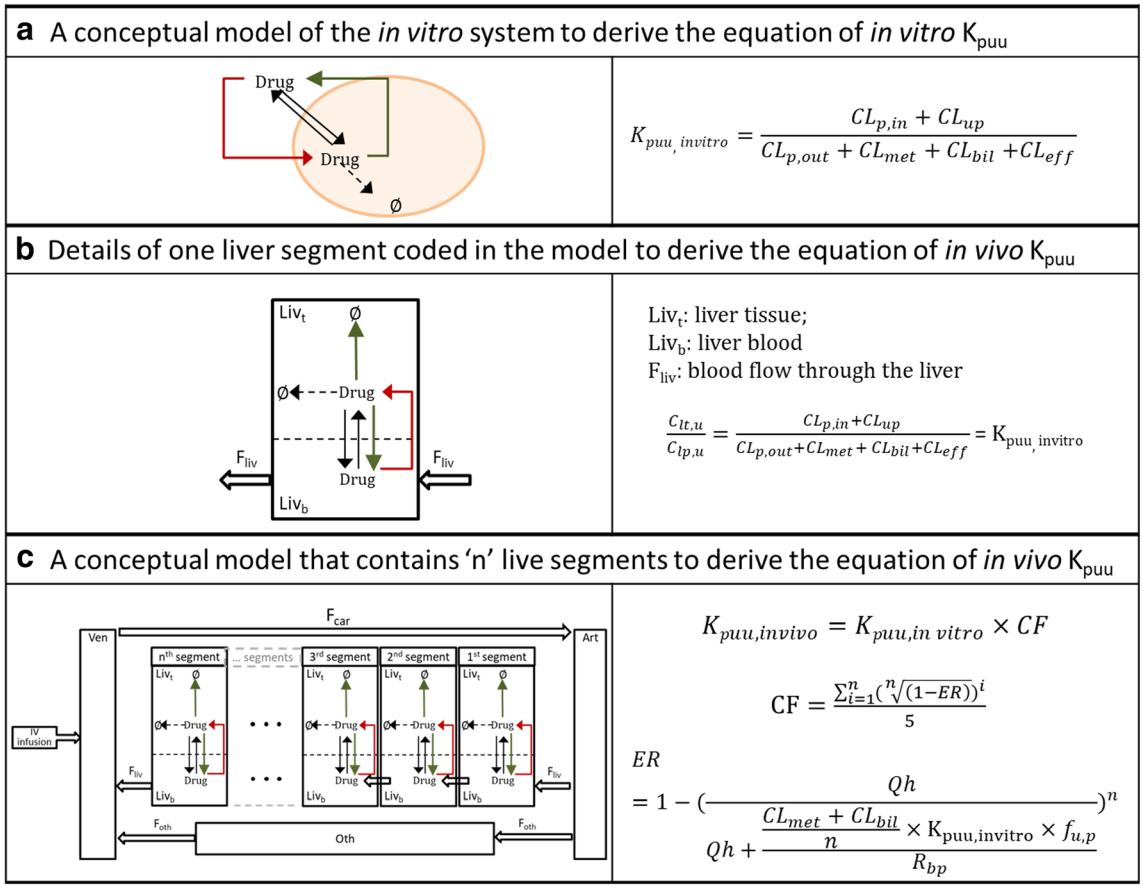

Fig. 1. Conceptual models and derived equations for K_{puu} calculation. **a** Equation derivation for *in vitro* K_{puu}. **b** Equation derivation for *in vivo* $K_{puu,app}$ using well-stirred model. **c** Equation derivation for *in vivo* $K_{puu,app}$ using five-compartment model

$$\frac{d(C_{ec} \times V_m)}{dt} + \frac{d(C_{ic} \times V_c)}{dt} = -CL_{met} \times C_{ic} \times f_{u,ic} = -K_{deg} \times (C_{ec} \times V_m + C_{ic} \times V_c) \quad (5)$$

$$k_{deg} = \frac{CL_{met} \times C_{ic} \times f_{u,ic}}{(C_{ec} \times V_m + C_{ic} \times V_c)} = \frac{CL_{met}}{\left(\frac{C_{ec} \times V_m}{C_{ic} \times f_{u,ic}} + \frac{V_c}{f_{u,ic}}\right)} = \frac{CL_{met}}{\left(\frac{V_m}{K_{puu,invitro} \times f_{u,ec}} + \frac{V_c}{f_{u,ic}}\right)} \quad (6)$$

$$-k_{deg} \times C_{ic} \times V_c = (CL_{p,in} + CL_{up}) \times C_{ec} \times f_{u,ec} - (CL_{p,out} + CL_{met} + CL_{bil} + CL_{eff}) \times C_{ic} \times f_{u,ic} \quad (7)$$

$$K_{puu,invitro} = \frac{CL_{p,in} + CL_{up}}{CL_{p,out} + CL_{met} + CL_{bil} + CL_{eff} - K_{deg} \times \frac{V_c}{f_{u,ic}}} = \frac{CL_{p,in} + CL_{up}}{CL_{p,out} + CL_{bil} + CL_{eff} + CL_{met} \times \left[1 - \frac{1}{\left(\frac{1}{K_{puu,invitro}} \times \frac{V_m}{V_c} \times \frac{f_{u,ic}}{f_{u,ec}} + 1\right)}\right]} \quad (8)$$

As a result, the difference between the PSS (Eq. 8) and the TSS (Eq. 4) $K_{puu,\ in\ vitro}$ depends upon the value of the expression within the brackets. As the value of this expression approaches 1, the PSS $K_{puu,\ in\ vitro}$ will approximate the value of TSS $K_{puu,\ in\ vitro}$. In order to appreciate the degree of difference, one can consider typical values for the parameters in the brackets. The ratio of V_m to V_c is assay dependent and approximately 700:1 for all compounds (*i.e.*, 0.5 million hepatocytes suspended in 1 mL of media). The ratio of $f_{u,\ ic}$ to $f_{u,\ ec}$ is typically ≥ 1 (since 4% BSA was added to the media in our studies). As a result, the effect of the term is negligible even when PSS $K_{puu,\ in\ vitro}$ is as high as 100 (*i.e.*, a value higher than observed to date in our experience).

Another consideration is that, given its value is always ≤ 1, the expression within the brackets of Eq. 8 has negligible influence when $CL_{met} << [CL_{p,out} + CL_{bil} + CL_{eff}]$, an assumption that is often made in determining intrinsic metabolic clearance rates in hepatocytes (*i.e.*, the rate of clearance is metabolic rate limited, not permeability limited). To further explore this relationship, we also used Eqs. 2 and 3 to generate simulations comparing TSS and PSS $K_{puu,\ in\ vitro}$ under a wide range of substrate depletion conditions (Supplementary Information 1). Based on these observations, hepatocyte measures of PSS $K_{puu,\ in\ vitro}$ (Eqs. 1 and 8) were assumed to adequately represent the TSS $K_{puu,\ in\ vitro}$ (Eq. 4) for this investigation.

Derivation of Mathematical Expressions for *In Vivo* K_{puu}

The equation of *in vivo* K_{puu} was derived based on conditions of an IV infusion to steady state. The *in vivo* K_{puu} was estimated as a ratio of two *in vivo* measurements, which are unbound drug concentrations in the liver tissue ($C_{lt,\ u}$) and the systemic plasma ($C_{sp,\ u}$) (Eq. 9). The fraction of unbound drugs in the liver ($f_{u,lt}$) and in the plasma ($f_{u,p}$) was measured to convert total concentrations to the unbound concentrations.

$$K_{puu,invivo} = \frac{C_{lt,u}}{C_{sp,u}} = \frac{C_{lt,t} \times f_{u,lt}}{C_{sp,t} \times f_{u,p}} \tag{9}$$

The model used to derive the equation of *in vivo* K_{puu} is a PBPK model that contains "*n*" permeability-limited liver segments, with each segment being further split into one liver tissue and one liver blood sub-compartment (Fig. 1b, c). The "*n*" segments represent the sequentially ordered hepatocytes in hepatic lobules, the basic building units of the liver composed of hepatocytes radiating outward from the central vein to the peri-portal region (15,16). Drugs are carried into the liver through the hepatic arterioles and the portal venules and then partition between liver blood and hepatocytes in each of the segments sequentially. The equation of *in vivo* K_{puu} was derived by examining passive permeation, active transport, and clearance rates in each segment.

The major assumption of this model and the corresponding derivation is that all the liver segments are equal in volume, blood flow, passive permeation, active transport, and clearance rates. Consequently, the *in vivo* observed ER is a result of a sequential extraction by the "n" liver segments. Secondly, we assumed that the measured unbound drug concentration in the liver is an average of unbound drug concentrations in the "n" liver segments ($C_{lt,\ u,\ i}$, $i = 1, 2 \cdots n$) (Eq. 10). This is a reasonable assumption, because samples of the liver tissue typically are big enough to contain all hepatocytes that form a hepatic lobule (*e.g.*, a hexagonal-shaped liver lobule is only about 1 mm in length (15). In addition, we did not consider enterohepatic recirculation (EHR) that may happen for biliary excreted drugs. Instead, we assumed that bile ducts functioned as a sink and drugs were eliminated once secreted, comparable to the conditions in the *in vitro* assay.

$$C_{lt,u} = \frac{\sum_{i=1}^{n} C_{lt,u,i}}{n}, \quad i = 1, 2, 3, \cdots n \text{ (number of segments)} \tag{10}$$

Based on this model, drug partition happens between the blood and the tissue sub-compartments within each liver segment. Equations 11 and 12 show the kinetics of drugs in liver tissue and liver blood sub-compartments of segment 1. At steady state, both Eqs. 11 and 12 equal 0. When Eq. 11 equals 0, the ratio between $C_{lt,\ u,\ 1}$ (*i.e.*, $C_{lt,\ 1} \times f_{u,\ lt}$) and the unbound drug concentration in the liver plasma ($C_{lp,\ u,\ 1}$, *i.e.*, $\frac{C_{lb,t,1} \times f_{u,p}}{R_{bp}}$) of segment 1 can be derived (Eq. 13), where R_{bp} represents the drug blood-to-plasma ratio and $C_{lb,\ t,\ 1}$ represents the total drug concentration in the liver blood sub-compartment of segment 1. Since each item of Eq. 13 is a function of the segment size, the effect of segment size is canceled out when the ratio is calculated. It is obvious that Eqs. 4 and 13 share the same mathematic formula, and the ratio of liver-to-plasma free drug concentrations in the segment equals the TSS *in vitro* K_{puu} (Eq. 4), because it is assumed that all passive permeation, active transport, and clearance rates per million hepatocytes are the same *in vitro* and *in vivo*.

$$\frac{dC_{lt,1} \times V_{lt,1}}{dt} = (CL_{p,in,1} + CL_{up,1}) \times \frac{C_{lb,t,1} \times f_{u,p}}{R_{bp}} - (CL_{p,out,1} + CL_{met,1} + CL_{bil,1} + CL_{eff,1}) \times C_{lt,1} \times f_{u,lt} \tag{11}$$

$$\frac{dC_{lb,t,1} \times V_{lb,1}}{dt} = Qh \times C_{sb,t} - (CL_{p,in,1} + CL_{up,1}) \times \frac{C_{lb,t,1} \times f_{u,p}}{R_{bp}} + (CL_{p,out,1} + CL_{eff,1}) \times C_{lt,1} \times f_{u,lt} - Qh \times C_{lb,t,1} \tag{12}$$

$$\frac{C_{lt,u,1}}{C_{lp,u,1}} = \frac{CL_{p,in,1} + CL_{up,1}}{CL_{p,out,1} + CL_{met,1} + CL_{bil,1} + CL_{eff,1}} = \frac{CL_{p,in} + CL_{up}}{CL_{p,out} + CL_{met} + CL_{bil} + CL_{eff}} = K_{puu,invitro,TSS} \tag{13}$$

When the sum of Eqs. 11 and 12 equals 0, it gives the ratio of the total drug concentration in liver blood of segment 1 to that in the systemic blood (Eq. 14), which is essentially ($1 - ER_1$).

$$1 - ER_1 = \frac{C_{lb,t,1}}{C_{sb,t}} = \frac{Qh}{Qh + \frac{(CL_{met,1} + CL_{bil,1}) \times K_{puu,invitro} \times f_{u,p}}{R_{bp}}} \tag{14}$$

Based on the assumption that each segment of the liver has the same passive and active uptake, passive and active efflux, as well as the same metabolic and biliary clearance rates, Eqs. 11 to 14 can be applied to liver segments 2 to n. The derivation suggests that ER_i $(i = 2, 3 \ldots n) = E_{sub} = ER_1$. The $C_{lp,\,u,\,i}$ in each segment can then be calculated using ER_{sub} (Eqs. 15 and 16). By substituting the unbound liver plasma drug concentrations, Eq. 17 can be derived to calculate the unbound drug concentrations in liver plasma that leave the liver and enter the venous pool. Equation 18 then solves the relationship between the ER and E_{sub}, and the unbound drug concentrations in liver plasma of segment i can be described as a function of those in systemic plasma using a general equation (Eq. 19).

$$C_{lp,u,1} = C_{sp,u} \times (1-ER_1) \tag{15}$$

$$C_{lp,u,i} = C_{lp,u,i-1} \times (1-ER_i), \quad i = 2-n \tag{16}$$

$$C_{lp,u,n} = C_{sp,u} \times (1-E_{sub})^n = C_{sp,u} \times (1-ER) \tag{17}$$

$$(1-E_{sub})^n = (1-ER) \tag{18}$$

$$C_{lp,u,i} = C_{sp,u} \times \left(\sqrt[n]{(1-ER)}\right)^i, \quad i = 1-n \tag{19}$$

Since it is assumed that each segment has the same passive permeation, active transport, and clearance rates, each liver segment shares the same liver-to-plasma free drug concentration ratio (Eq. 20). It is obvious that the right side of Eq. 20 is the same as that in Eqs. 4 and 13, identical to TSS *in vitro* K_{puu}. As a result, the unbound liver tissue concentration can be described using Eq. 21.

$$\frac{C_{lt,u,1}}{C_{lp,u,1}} = \frac{C_{lt,u,2}}{C_{lp,u,2}} = \ldots = \frac{C_{lt,u,i}}{C_{lp,u,i}} = \frac{CL_{p,in} + CL_{up}}{CL_{p,out} + CL_{met} + CL_{bil} + CL_{eff}} = K_{puu,invitro,TSS} \tag{20}$$

$$C_{lt,u,i} = C_{lp,u,i} \times K_{puu,invitro} \quad i = 1-n \tag{21}$$

The *in vivo* K_{puu} can then be represented using Eq. 22 as a function of *in vitro* K_{puu}. By substituting Eq. 19 into Eq. 22, the formula is further simplified to Eq. 23. In Eq. 23, the term in the brackets can be viewed as a correction factor (CF) that translates $K_{puu,in\ vitro}$ to $K_{puu,in\ vivo}$. The CF is a function of ER as well as "n," the number of liver segments coded in the model. If ER is zero (*i.e.*, the liver does not serve as an elimination organ), CF equals one regardless of the value of n. When ER is non-zero and n approaches infinity (*e.g.*, similar to parallel tube model but considers the asymmetric drug distribution into the hepatocytes), the limit of CF can be derived in Eq. 24 using MATLAB® R2017b.

$$K_{puu,invivo} = \frac{C_{lt,u}}{C_{sp,u}} = \frac{\sum_{i=1}^{n} C_{lt,u,i}}{n \times C_{sp,u}} = K_{puu,invitro} \times \left(\frac{\sum_{i=1}^{n} C_{lp,u,i}}{n \times C_{sp,u}}\right) \tag{22}$$

$$K_{puu,invivo} = K_{puu,invitro} \times \left[\frac{\sum_{i=1}^{n}\left(\sqrt[n]{(1-ER)}\right)^i}{n}\right] \tag{23}$$

$$K_{puu,invivo} = K_{puu,invitro} \times \left[\frac{-ER}{Ln(1-ER)}\right] \tag{24}$$

To better understand how ER and "n" coded in the model affect the value of CF, simulations were conducted in MATLAB® R2017b by varying n from one to infinity and ER from 0 to 0.999.

Prediction of *In Vivo* K_{puu} Using *In Vitro* K_{puu} and *In Vivo* ER from Literature

To examine the predictive power of the equations, we applied the derived Eq. 24 to reported literature information regarding the observed *in vitro* and *in vivo* K_{puu} for nine compounds in rats and two compounds in humans (2,3). For each compound, ER was either obtained from literature or calculated based upon *in vivo* hepatic clearance from publication. The reported *in vitro* K_{puu} and *in vivo* ER were inserted into Eq. 24 to predict *in vivo* K_{puu} which were then used to compare to the reported *in vivo* K_{puu} measurements.

Derivation of Mathematical Expressions for ER

As CF is a function of ER, we further derived equations to calculate ER from *in vitro* data, with the same "n"-segment liver model used to derive the K_{puu} equations. By cominbing Eqs. 14 and 18, ER can be expressed as shown in Eq. 25, where CL_{met} and CL_{bil} refer to the metabolic and biliary clearance rates for the whole liver. For example, if the *in vitro* metabolic rate is measured in units of microliter per minute per million hepatocytes, the CL_{met} for a whole liver can be calculated by multiplying the *in vitro* rate with the total number of hepatocytes in the liver. Since "n" represents the number of segments coded in the model, in each segment, the metabolic clearance will be $\frac{CL_{met}}{n}$. Further, the same holds for CL_{bil}. When "n" approaches ∞, the model performs similarly

to a parallel tube model but considers the asymmetric drug distribution in the liver tissue, and the limit can be solved in MATLAB® R2017b, which is an exponential function as shown in Eq. 26. The difference between this formula and the one from traditional parallel tube model is that Eq. 26 considers the potential of asymmetric intracellular drug concentrations using K_{puu}.

$$ER = 1 - \left(\frac{Qh}{Qh + \frac{\frac{CL_{met}+CL_{bil}}{n} \times K_{puu,invitro} \times f_{u,p}}{R_{bp}}} \right)^{n} \quad (25)$$

$$ER = 1 - \exp\left(- \frac{(CL_{met} + CL_{bil}) \times K_{puu,invitro} \times f_{u,p}}{Qh \times R_{bp}} \right) \quad (26)$$

Apparently, ER is also a function of "*n*," the number of liver segments coded in the model. To better understand how "*n*" (*i.e.*, different liver models) affects ER estimation, simulations were conducted in MATLAB® R2017b by varying *n* from one to infinity. Since the purpose of this simulation is to explore the effect of "*n*," the clearance parameters ($CL_{met} + CL_{bil}$) and $K_{puu,in\ vitro}$ were lumped as one (essentially intrinsic clearance rate). In addition, both the values of $f_{u,p}$ and R_{bp} were fixed to one for simplicity.

Effects of Zonal Distribution of Liver Enzymes on *In Vivo* K_{puu}

The above derivations were based upon an assumption that all the liver segments function equally. However, major drug metabolism enzymes like UGTs and CYPs have been reported to locate mainly at the peri-venous region around the central venin (16). To explore how assumptions of this nature affect *in vivo* K_{puu} and ER estimation, we coded a five-segment liver model (7,8) in MATLAB® R2017 b and simulated the effect by assuming metabolic enzymes are (1) mainly at the peri-portal region, (2) evenly distributed, and (3) mainly at the peri-venous region. All three conditions were simulated for two cases: (1) CL_{met} being a small contributor to *in vitro* K_{puu} and (2) CL_{met} being a big contributor of *in vitro* K_{puu}. All the model parameters used in these simulations are listed in Table I, where $CL_{p,in}$ and $CL_{p,out}$ were assumed to have the same value. In Supplementary Information 2, we repeated the simulation of the two cases by assigning $CL_{p,in}$ to a value that equals 5- or 0.2-fold of $CL_{p,out}$ to explore potential effects.

RESULTS

Simulation Results of the CF as a Function of both ER and "*n*" Coded in the Model

The simulation results of CF as a function of ER and "*n*" are presented in Fig. 2a. As previously illustrated, when ER is zero (*i.e.*, the liver does not serve as the clearance organ), no matter how many liver segments were coded in the model, the CF equals one (*i.e.*, *in vitro* K_{puu} = *in vivo* K_{puu}). However, as long as ER is a non-zero, CF is a function of both ER and "*n*." When ER is low, CF is relatively insensitive to the value of "*n*" (*e.g.*, 0.95–0.97 when ER = 0.05). At the other extreme, CF is highly sensitive to "*n*" when ER is very high (*e.g.*, 0.01–0.21 when ER = 0.99). However, the practical relevance of this observation is likely to be limited, because the K_{puu} for compounds with such a high ER are rarely examined since they are unlikely to advance along the drug discovery pipeline. At moderate ER values, CF is modestly sensitive to *n* (*e.g.*, 0.5–0.72, when ER = 0.5). Given that the CF is within twofold of unity over much of the moderate ER range, it is unlikely to seriously confound the direct correlation between *in vitro* and *in vivo* K_{puu}.

Simulation Results of the ER as a Function of "*n*" Coded in the Model

The effects on ER prediction by the number of liver segments coded in the model are presented in Fig. 2b. When intrinsic clearance rate (*i.e.*, $(CL_{met} + CL_{bil}) \times K_{puu,in\ vitro}$) is low (*e.g.*, < 10 mL/min/kg), the ER prediction is not sensitive to the number of liver segments. However, the sensitivity increases with the increasing intrinsic clearance rate, and the maximal sensitivity shows up when intrinsic clearance rate is around 50 to 100 mL/min/kg. After that, the sensitivity decreased again. This is because the maximal prediction of ER approaches a value of one for all models when intrinsic clearance rate is high enough.

Comparison of Predicted and Observed In Vivo K_{puu}

The predicted *in vivo* K_{puu} using models that contain 1, 5, or an infinite number of liver segments were summarized in Table II. When ER is high, the results from models that contain a higher number of liver segments (*e.g.*, infinity) are more consistent with previous reports that demonstrate a good IVIVE (2,3). The three compounds from Riccardi *et al.* (2) are metabolically stable with low ER, leading to a successful translation no matter how many liver segments were coded. Riccardi *et al.* (3) evaluated the translation of K_{puu} from *in vitro* to *in vivo* in both human and rats. In human, the hepatic ER of rosuvastatin and pravastatin were reported in a range from 0.3 to 0.6 (19,20), indicating a negligible CF in the context of the experimental variability. Based upon the total plasma clearance calculation, three out of six compounds (cerivastatin, fluvastatin, and PF-04991532) evaluated in Riccardi *et al.* have hepatic ER less than 0.3 in rats (*e.g.*, total plasma clearance less than 1/3 of hepatic plasma flow), leading to a negligible CF. Pravastatin has a hepatic ER of 0.7 in rats (21), with which the one-segment liver model predicts a CF of 0.3 and the infinite-segment liver model predicts a CF about 0.6 (a twofold difference between the two models). Rosuvastatin has a hepatic ER ranging from 0.42 (22) to 0.93 in rats (23). With this degree of extraction, the one-segment liver model predicts a CF of 0.07 to 0.58, while the infinite-segment liver model predicts a CF around 0.35 to 0.77 (a fivefold difference between the two models if ER is 0.93). The compound, PF-05187965, has a very high blood clearance, greater than the hepatic blood flow in rats (0.29 mL/s), an observation that confounds the current analysis to some degree. However, according to the infinite-

Table I. Parameters Used in the Five-Compartment Model to Simulate the Effects of Enzyme Zonation

Parameter	Symbols	Values 1[a]	Values 2[b]	Units	Reference
Hepatic blood flow	Q_h	25	25	mL/min/kg	(7,8)
Systemic total blood concentration	$C_{sb,t}$	1	1	μM	Fixed as IV infusion
Passive permeation clearance into the liver	$CL_{p,in}$	50	5	mL/min/kg	(7,8)
Passive permeation clearance out the liver	$CL_{p,out}$	50	5	mL/min/kg	(7,8)
Active uptake clearance into the liver	CL_{up}	2000	200	mL/min/kg	(7,8)
Active efflux clearance out the liver	CL_{eff}	50	5	mL/min/kg	(7,8)
Total metabolic clearance	CL_{met}	10	100	mL/min/kg	(7,8)
Ratio of $CL_{met,i}$ among compartments	F_{diff}	1	1	–	Varied [0.25, 1, 4]
Fraction of unbound in the plasma	f_{up}	1	1	–	Assumed
Fraction of unbound in the liver	f_{ul}	1	1	–	Assumed
Blood plasma ratio	R_{bp}	1	1	–	Assumed
Volume of liver blood	V_{lb}	0.33	0.33	L	(7,8)
Volume of liver tissue	V_{lt}	1.8	1.8	L	(7,8)
In vitro K_{puu}	–	18.6	1.86	–	Calculated
Total intrinsic clearance	CL_{int}	186	186	mL/min/kg	Calculated

[a] Values of parameter set 1 that defines the CL_{met} as 10 mL/min/kg and the *in vitro* K_{puu} as 18.6. The simulation results from these parameter values are presented in Fig. 3a–c

[b] Values of parameter set 2 that defines the CL_{met} as 100 mL/min/kg and the *in vitro* K_{puu} as 1.86. The simulation results from these parameter values are presented in Fig. 3d–f

segment liver model, the CF is only 0.22 even if the ER is as high as 0.99; in contrast, a one-segment liver model predicts a CF of 0.01 (a 22-fold difference between the two models). Here, it is interesting to note that the reported *in vitro* K_{puu} of this compound was greater than that of the *in vivo* measurement (*i.e.*, 4.2 vs 2.4), directionly consistent with the model prediction.

Simulation of the Effects on K_{puu} Translation by Metabolic Zonation in the Liver Segments

To simplify the equation derivations, we assumed that all liver segments in the model functioned equally with the same E_{sub}. This hypothesis has been used in literature for five-liver-segment PBPK models as well as the traditional parallel tube models (7,8,18). However, depending on the enzymes, some demonstrate a zonal distribution. For example, it has been reported that CYP and glucuronidation, two major drug-metabolizing enzymes, are mainly in the peri-venous region around the central vein (16).

The effects of zonal distribution of metabolic enzymes were explored by simulating the five-liver-segment model, and the results indicate that the *in vitro* K_{puu} can better represent *in vivo* K_{puu} (Fig. 3a–c) when the clearance mainly distributes at the peri-venous region, when CL_{met} is not the determining factor of *in vitro* K_{puu}. This is not surprising when the drug concentration in the liver plasma sub-compartment ($C_{lp,u}$) is considered. Figure 3a shows an immediate drop of $C_{lp,u}$ when intrinsic clearance was mainly at the peri-portal region. In contrast, $C_{lp,u}$ was maintained at a high level similar to that in the systemic circulation until the drug reached the metabolic enzyme at the peri-venous region (Fig. 3c). Since *in vivo* K_{puu} is the ratio between $C_{lt,u}$ and $C_{sp,u}$ and *in vitro* K_{puu} is closer to the ratio of $C_{lt,u}$ and $C_{lp,u}$, it is not surprising to see that *in vitro* K_{puu} represents *in vivo* K_{puu} better when $C_{lp,u}$ is closer to $C_{sp,u}$ (*i.e.*, clearance mainly occurs around the central vein). When metabolic clearance is a big contributor of *in vitro* K_{puu}, the values of *in vitro* K_{puu} should be relatively low since drugs that distribute into the tissue are cleared fast and cannot accumulate. Under such conditions, the simulated *in vivo* K_{puu} is a result of interplay between the plasma-tissue partition and the CL_{met} (Fig. 3d–f). With the current parameterization, the *in vivo* K_{puu} was predicted to be greater than one only when enzymes are mainly located at the peri-venous region (Fig. 3f), comparable to the *in vitro* K_{puu} (4.6 vs 1.86). Changing the ratio between $CL_{p,in}$ and $CL_{p,out}$ values did not change the above observations and conclusions (Supplementary Information 2).

DISCUSSION

Hypothesis About Enzyme and Transporter Activities in the *In Vitro* System

To explore the theoretical basis for direct translation of K_{puu} from *in vitro* to *in vivo*, we made a hypothesis that all the hepatic enzymes and transporters in the *in vitro* system were functioning the same as those *in vivo*. The hypothesis is based upon experimental data obtained under our assay conditions (*e.g.*, 4% BSA in InVitroGRO HI media), which showed a strong *in vitro* and *in vivo* correlation of liver K_{puu} (2,3,24). This suggests that the *in vitro* system is likely to function similarly to *in vivo* in terms of drug-metabolic enzymes and transporters. It is important to note that *in vitro* assay conditions are critical to assess *in vivo* performance. Certain conditions, such as plated hepatocytes without BSA or plasma, tend to under-predict *in vivo* OATP transport and metabolic functions, leading to the necessity of using empirical scaling factors (7).

The CF derived in this study reflects the theoretical differences between *in vitro* and *in vivo* measured K_{puu} (*i.e.*, if the same parameters were measured *in vitro* and *in vivo*), while it does not account for potential differences in enzyme and/or transporter activities. Empirical scaling factors (7,8)

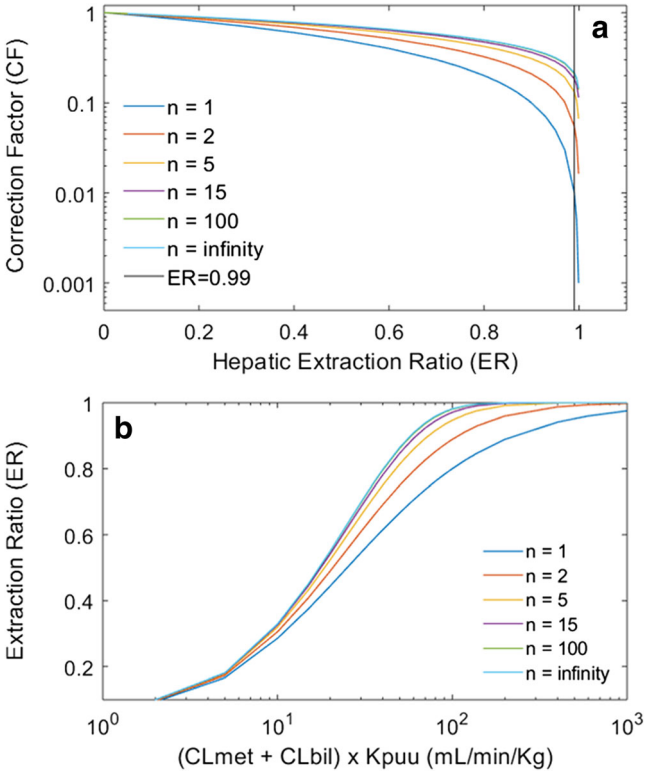

Fig. 2. Simulation results of CF as a function of both ER and "*n*," the number of liver segments coded in the model. When ER is low, CF is not sensitive to "*n*"; however, the sensitivity increases with increasing ER. When ER is 0.99, the model with one liver segment predicts a CF of 0.01; in contrast, the model with 100 or infinity number of liver segments predicts a CF of 0.21. Majority PBPK models contain only one liver segment, including the extended clearance model (17). The permeability-limited five-liver-segment PBPK model has also been used in the industry (7,8). The traditional parallel tube model treats the liver as a tube that essentially contains infinity number of liver segments (18) but does not consider the asymmetric drug distribution in the liver tissue. We updated the parallel tube model to include this feature in this study

typically either refer to the differences in enzyme/transporter activities or lump all the differences between *in vitro* and *in vivo* systems together in a composite value.

From another side, our simulation results indicate that there should be some room to further improve our *in vitro* K_{puu} assay, that is, hepatic enzyme and/or transporter activities might be further optimized. According to the models, the *in vitro* measured K_{puu} should always be equal to (*e.g.*, the liver does not serve as an elimination organ) or great than (*e.g.*, the liver serves as an elimination organ) the *in vivo* K_{puu} if all passive permeation, active transport, and clearance rates are the same *in vitro* and *in vivo*. This is because (1) Eq. 8 will always be ≥ Eq. 4, although we have proved that the values of Eqs. 8 and 4 are very close and, (2) in Eq. 23, the CF converting the *in vitro* K_{puu} to the *in vivo* is always ≥ 1. However, the majority of the compounds listed in Table II have measured *in vitro* K_{puu} values smaller than those measured *in vivo*. After applying Eqs. 23 and 24, the predicted *in vivo* K_{puu} values are even smaller. For example, rosuvastatin had a measured *in vitro* K_{puu} of 35 in rats; the predicted *in vivo* K_{puu} ranged from 12 to 27 using the updated parallel tube model and even smaller values using the models with 1 or 5 liver segments. Compared to the measured *in vivo* K_{puu} of 57, the measured *in vitro* K_{puu} seems more accurate but is still lower than the *in vivo* measurement.

Limitations of the Current Analysis

When it comes to more complicated research topics, *e.g.*, non-steady-state tissue-to-plasma concentration ratio, a full PBPK model should be a better way to simulate the effects, other than algebraic equations derived at TSS *in vivo* or PSS *in vitro* in this analysis. In reality, most pharmaceuticals are dosed as either IV or PO boluses rather than IV infusion. The time-dependent profile of the non-steady-state tissue-to-plasma concentration ratio is more useful than steady-state K_{puu} to predict the downstream efficacy or toxicity.

Table II. Comparison of Model-Predicted *In Vivo* K_{puu} to the Observations

Compounds	*Observed in vitro* K_{puu}[a]	Observed *in vivo* ER[a]	Observed *in vivo* K_{puu}[a]	Predicted *in vivo* K_{puu}[b]		
				Number of liver segments		
				Infinity	5	1
Rats						
PF-06649298	14 ± 2.6	Minimal	16 ± 1.3	14	14	14
PF-06649297	0.5 ± 0.2	Minimal	2.4 ± 0.6	0.5	0.5	0.5
PF-06761281	1.5 ± 0.3	Minimal	1.7 ± 0.4	1.5	1.5	1.5
Cerivastatin	21 ± 2.0	< 0.3	29 ± 8.5	> 18	> 17	> 15
Fluvastatin	22 ± 1.5	< 0.3	44 ± 8.7	> 19	> 18	> 15
Rosuvastatin	35 ± 0.6	0.42 (20)–0.93(21)	57 ± 9.5	12–27	9.3–25	2.5–20
Pravastatin	3.0 ± 0.3	0.7 (19)	2.2 ± 1.5	1.7	1.5	0.9
PF-04991532	7.1 ± 0.1	< 0.3	5.7 ± 1.6	> 6.0	> 6	> 5
PF-05187965	4.2 ± 0.2	~ 0.99	2.4 ± 0.57	~ 0.9	~ 0.5	~ 0.04
Humans						
Rosuvastatin	39 ± 5.0	0.36 (18)–0.63 (17)	10	25–31	22–30	14–36
Pravastatin	2.3 ± 0.2	0.31 (18)	2.0 to 5.3	1.9	1.9	1.6

[a] Data are summarized from paper (2,3)
[b] Predictions are calculated from *in vitro* K_{puu} and *in vivo* ER using the CF from models that contain one, five, and infinity number of liver segments

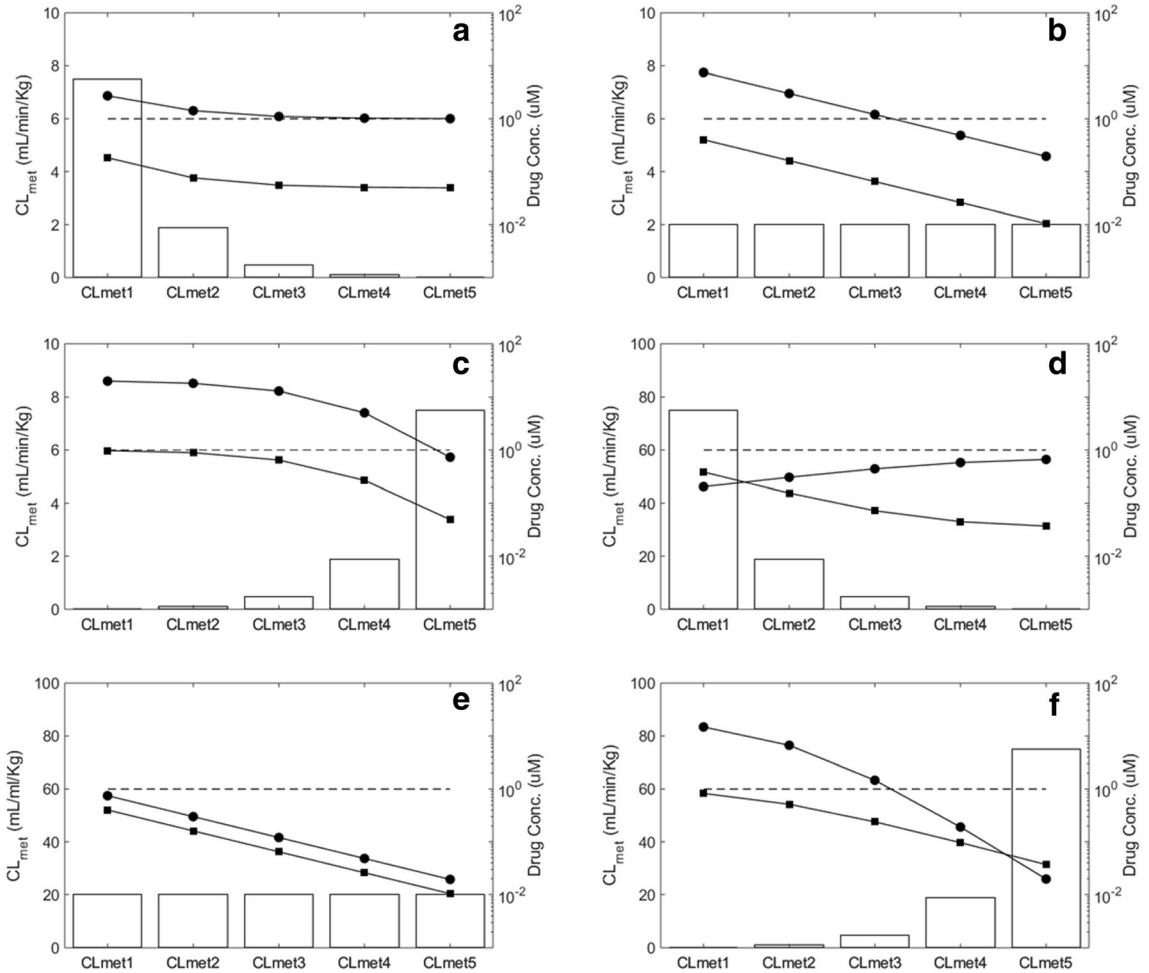

Fig. 3. Simulation results of the effects of enzyme zonation. For all simulations, the total CL_{int} is 186 mL/min/kg. For panels **a**–**c**, the CL_{met} is 10 mL/min/kg and the *in vitro* K_{puu} is 18.6. For panels **d**–**f**, the CL_{met} is 100 mL/min/kg and the *in vitro* K_{puu} is 1.86. For panels **a** and **d**, metabolic clearance locates mainly at the peri-portal region. The ratio of metabolic clearance in compartment i to that in compartment $i+1$ equals 4 ($i = 1, 2, \ldots 5$). For panels **b** and **e**, metabolic clearance distributes evenly. For panels **c** and **f**, metabolic clearance locates mainly at the peri-venous region. The ratio of metabolic clearance in compartment i to that in compartment $i+1$ equals 0.25 ($i = 1,2,\ldots 5$). The *in vivo* $K_{puu,app}$ was simulated to be 1.5 in panel **a**, 2.5 in panel **b**, 11.4 in panel **c**, 0.44 in panel **d**, 0.25 in panel **e**, and 4.6 in panel **f**

Quantitatively, the non-steady-state ratios could be quite different from the steady-state K_{puu}. For example, in a PO study, drug is first absorbed into the portal vein and then distributed into the liver and subsequently the systemic blood; as such, drug in the portal vein could contribute significantly to the liver drug pool in addition to the systemic blood. Depending on the absorption rate constant and dosing amount, this could lead to an apparent "K_{puu}" that is significantly higher than the one measured at the steady state following an IV infusion.

Another limitation of this exercise is that we assumed no EHR *in vivo* or the magnitude was small and negligible. This simplified the questions to be addressed and helped the equation derivation. However, EHR does happen for some drugs that undergo biliary excretion. During the process, biliary drug is secreted into the gut and some fraction of this is then reabsorbed into the portal vein, forming another source of drug in addition to the systemic blood. As such, the observed *in vivo* "K_{puu}" could be much higher, with the degree of "K_{puu}" increase determined by the fraction and the rate of the drug reabsorption into the portal vein.

Given the degree of complexity of the above two cases (*i.e.*, PO and EHR), a full PBPK model should be a better way to simulate the effects, other than algebraic equations. However, parameters in Eqs. 11 and 12 are needed in order to run these simulations. Based on the current analysis, the *in vitro* assay predicted *in vivo* K_{puu} well and has a theoretical basis, indicating that the assay may indeed capture *in vivo* enzyme and transporter activities to a reasonable degree. Experiments using the assay can be designed to tease out the value of each parameter in Eqs. 11 and 12, which can then be inserted in full PBPK models to predict *in vivo* non-steady-state PK profiles that are more meaningful in the context of efficacy or toxicity predictions.

Models and Updated Models in This Study

A model that contains "n" permeability-limited liver segments was explored in this study, and we specifically

focused on models with one, five, or an infinite number of liver segments. The one-segment liver model is essentially a permeability-limited well-stirred liver model that is well accepted and widely used in PBPK models (25). The five-segment liver model is used much less frequently but still considered as a general practice and has been applied in the industry (7,8). In contrast, there is almost no implementation of parallel tube model in a PBPK setting, probably because it treats the liver as a tube that essentially contains an infinite number of segments and is lack of a flexibility to study the inside of the liver. However, the traditional parallel tube model has been demonstrated to have advantages over the others when converting *in vivo* CL_h to CL_{int} (25).

The major purpose of this study is to understand the theoretical basis of translating *in vitro* measured K_{puu} (of hepatocytes to media) to *in vivo* (of the liver to the systemic plasma). To do so, we examined and updated a couple of traditional liver models using the permeability-limited concept. The traditional PBPK models with a flow-limited liver compartment (*e.g.*, a well-stirred liver model (25)) use Kp (*i.e.*, the ratio of total drug concentration in the liver to that in the venous blood leaving the liver) to calculate liver drug concentrations and assume that the ratio of each drug holds constantly even at non-steady state, which may not be true for poor permeable compounds. In the updated models, we treated drug distribution in each liver segment as a permeability-limited process, allowing us to simulate the dynamic profile of the liver to blood drug concentration ratio. There are publications of the extended clearance model (17), which holds a concept similar to the equation we derived from the one-segment liver model (*i.e.*, permeability-limited well-stirred liver model) (25). However, we are not aware of any publication that gives the equations for the five-segment liver model or infinite number of liver segments (*i.e.*, permeability-limited parallel tube model).

It is very interesting to see that, when the number of liver segments "n" is ≥ 15, both ER and CF are insensitive to "n" (Fig. 2). In reality, typically there are 15 to 20 hepatocytes along the radius of each hepatic lobule (15,16). If we use one liver segment in the model to represent the micro-environment that contains one hepatocyte (*e.g.*, liver tissue sub-compartment coded in the model) and its surrounding interstitial fluid (*e.g.*, liver blood sub-compartment coded in the model), we basically have little need to correct for apparent differences between *in vitro* and *in vivo* K_{puu} (*i.e.*, CF is only 0.36 even if the ER is as high as 0.9). Also, as shown in (Fig. 2), the ER prediction from a model that has 15 liver segments is very similar to those predicted by models that contain 100 or an infinite number of liver segments.

CONCLUSION

This study provides the theoretical basis for direct translation of the K_{puu} from *in vitro* to *in vivo*. Most compounds of high interest in drug discovery are likely to have low to moderate ER. Even for compounds with ER values as high as 0.9, CF estimated from models that contain 15 or more number of liver segments ranges from 0.36 to 0.39, suggesting a less than threefold difference between *in vitro* and *in vivo* K_{puu}. Such a small difference is not likely to be very significant considering experimental variability. In addition, this study also suggests that models that contain 15 to an infinite number of liver segments (*i.e.*, permeability-limited parallel tube model) are perhaps the most appropriate PBPK construct to support studies of this nature.

ACKNOWLEDGEMENTS

The authors would like to acknowledge Karen Atkinson for editing the manuscript.

REFERENCES

1. Mateus A, Matsson P, Artursson P. Rapid measurement of intracellular unbound drug concentrations. Mol Pharm. 2013;10(6):2467–78.
2. Riccardi K, Li Z, Brown Janice A, Gorgoglione Matthew F, Niosi M, Gosset J, et al. Determination of unbound partition coefficient and in vitro-in vivo extrapolation for SLC13A transporter-mediated uptake. Drug Metab Dispos. 2016;44(10):1633–42.
3. Riccardi K, Lin J, Li Z, Niosi M, Ryu S, Hua W, et al. Novel method to predict in vivo liver-to-plasma Kpuu for OATP substrates using suspension hepatocytes. Drug Metab Dispos. 2017;45(5):576–80.
4. Shitara Y, Maeda K, Ikejiri K, Yoshida K, Horie T, Sugiyama Y. Clinical significance of organic anion transporting polypeptides (OATPs) in drug disposition: their roles in hepatic clearance and intestinal absorption. Biopharm Drug Dispos. 2013;34(1):45–78.
5. Yabe Y, Galetin A, Houston JB. Kinetic characterization of rat hepatic uptake of 16 actively transported drugs. Drug Metab Dispos. 2011;39(10):1808–14.
6. Zhang D, Luo G, Ding X, Lu C. Preclinical experimental models of drug metabolism and disposition in drug discovery and development. Acta Pharm Sin B. 2012;2(6):549–61.
7. Li R, Barton HA, Yates PD, Ghosh A, Wolford AC, Riccardi KA, et al. A "middle-out" approach to human pharmacokinetic predictions for OATP substrates using physiologically-based pharmacokinetic modeling. J Pharmacokinet Pharmacodyn. 2014;41(3):197–209.
8. Jones HM, Barton HA, Lai Y, Bi Y-A, Kimoto E, Kempshall S, et al. Mechanistic pharmacokinetic modeling for the prediction of transporter-mediated disposition in humans from sandwich culture human hepatocyte data. Drug Metab Dispos. 2012;40(5):1007–17.
9. Morse BL, Cai H, MacGuire JG, Fox M, Zhang L, Zhang Y, et al. Rosuvastatin liver partitioning in cynomolgus monkeys: measurement in vivo and prediction using in vitro monkey hepatocyte uptake. Drug Metab Dispos. 2015;43(11):1788–94.
10. Kunze A, Huwyler J, Camenisch G, Poller B. Prediction of organic anion-transporting polypeptide 1B1- and 1B3-mediated hepatic uptake of statins based on transporter protein expression and activity data. Drug Metab Dispos. 2014;42(9):1514–21.
11. Badee J, Achour B, Rostami-Hodjegan A, Galetin A. Meta-analysis of expression of hepatic organic anion-transporting polypeptide (OATP) transporters in cellular systems relative to human liver tissue. Drug Metab Dispos. 2015;43(4):424–32.
12. Li M, Yuan H, Li N, Song G, Zheng Y, Baratta M, et al. Identification of interspecies difference in efflux transporters of hepatocytes from dog, rat, monkey and human. Eur J Pharm Sci. 2008;35(1–2):114–26.
13. Bow DA, Perry JL, Miller DS, Pritchard JB, Brouwer KL. Localization of P-gp (Abcb1) and Mrp2 (Abcc2) in freshly isolated rat hepatocytes. Drug Metab Dispos. 2008;36(1):198–202.
14. Lundquist P, Englund G, Skogastierna C, Lööf J, Johansson J, Hoogstraate J, et al. Functional ATP-binding cassette drug

efflux transporters in isolated human and rat hepatocytes significantly affect assessment of drug disposition. Drug Metab Dispos. 2014;42(3):448–58.
15. Teutsch HF. The modular microarchitecture of human liver. Hepatology. 2005;42(2):317–25.
16. Kietzmann T. Metabolic zonation of the liver: the oxygen gradient revisited. Redox Biol. 2017;11:622–30.
17. Camenisch G, Riede J, Kunze A, Huwyler J, Poller B, Umehara K. The extended clearance model and its use for the interpretation of hepatobiliary elimination data. ADMET and DMPK 2015.
18. Pang KS, Rowland M. Hepatic clearance of drugs. I. Theoretical considerations of a "well-stirred" model and a "parallel tube" model. Influence of hepatic blood flow, plasma and blood cell binding, and the hepatocellular enzymatic activity on hepatic drug clearance. J Pharmacokinet Biopharm. 1977;5(6):625–53.
19. Martin PD, Warwick MJ, Dane AL, Brindley C, Short T. Absolute oral bioavailability of rosuvastatin in healthy white adult male volunteers. Clin Ther. 2003;25(10):2553–63.
20. Shitara Y, Horie T, Sugiyama Y. Transporters as a determinant of drug clearance and tissue distribution. Eur J Pharm Sci. 2006;27(5):425–46.
21. Yamazaki M, Kobayashi K, Sugiyama Y. Primary active transport of pravastatin across the liver canalicular membrane in normal and mutant Eisai hyperbilirubinemic rats. Biopharm Drug Dispos. 1996;17(7):607–21.
22. Lundquist P, Loof J, Fagerholm U, Sjogren I, Johansson J, Briem S, et al. Prediction of in vivo rat biliary drug clearance from an in vitro hepatocyte efflux model. Drug Metab Dispos. 2014;42(3):459–68.
23. Iusuf D, van Esch A, Hobbs M, Taylor M, Kenworthy KE, van de Steeg E, et al. Murine Oatp1a/1b uptake transporters control rosuvastatin systemic exposure without affecting its apparent liver exposure. Mol Pharmacol. 2013;83(5):919–29.
24. Mao J, Doshi U, Wright M, Hop CECA, Li AP, Chen Y. Prediction of the pharmacokinetics of pravastatin as an OATP substrate using plateable human hepatocytes with human plasma data and PBPK modeling. CPT Pharmacometrics Syst Pharmacol. 2018;7(4):251–8.
25. Ito K, Houston JB. Comparison of the use of liver models for predicting drug clearance using in vitro kinetic data from hepatic microsomes and isolated hepatocytes. Pharm Res. 2004;21(5):785–92.